

# A coupled-trajectory quantum-classical approach to electronic decoherence in non-adiabatic processes

Seung Kyu Min,<sup>1,2</sup> Federica Agostini,<sup>1</sup> and E. K. U. Gross<sup>1</sup>

<sup>1</sup>Max-Planck Institut für Mikrostrukturphysik, Weinberg 2, D-06120 Halle, Germany

<sup>2</sup>Department of Chemistry, School of Natural Science,

Ulsan National Institute of Science and Technology (UNIST), Ulsan 689-798, Korea

(Dated: October 12, 2018)

We present a novel quantum-classical approach to non-adiabatic dynamics, deduced from the coupled electronic and nuclear equations in the framework of the exact factorization of the electron-nuclear wave function. The method is based on the quasi-classical interpretation of the nuclear wave function, whose phase is related to the classical momentum and whose density is represented in terms of classical trajectories. In this approximation, electronic decoherence is naturally induced as effect of the coupling to the nuclei and correctly reproduces the expected quantum behaviour. Moreover, the splitting of the nuclear wave packet is captured as consequence of the correct approximation of the time-dependent potential of the theory. This new approach offers a clear improvement over Ehrenfest-like dynamics. The theoretical derivation presented in the Letter is supported by numerical results that are compared to quantum mechanical calculations.

PACS numbers: 31.15.-p, 31.50.-x, 31.15.xg, 31.50.Gh, 82.20.Gk

The theoretical description of phenomena such as vision [1], photo-synthesis [2], photo-voltaic processes [3], proton-transfer and hydrogen storage [4] is among the most challenging problems in Condensed Matter Physics and Theoretical Chemistry. The underlying quantum dynamics of electrons and nuclei exhibit a non-adiabatic character, meaning that it cannot be explained by employing the Born-Oppenheimer (BO) approximation. In this respect, the major challenge for theory resides in the explicit treatment of electronic excited-state dynamics coupled to the nuclear motion. While methods that retain quantum features of the nuclear dynamics [5] are the most accurate to address this problem, they cannot be applied to systems with hundreds, or even thousands, of atoms. Therefore, a treatment of nuclear dynamics in terms of (semi)classical trajectories [5–9] represent the most promising and numerically feasible approach for actual calculations. Despite the great effort that has been devoted over the years to the development of such methods, actual applications are still limited [10]. Well-known issues are connected to the lack of, or incorrect account for, decoherence and to the inability of reproducing the spatial splitting of a nuclear wave packet, as in Ehrenfest-like dynamics. In the study of electronic non-adiabatic processes, these problems can result in wrong predictions for quantum populations and in unphysical outcomes for the nuclear dynamics.

We have recently proposed a new formalism that can be employed to overcome the above issues, the so-called exact factorization of the electron-nuclear wave function [11]. In this framework, the full wave function is written as the product of a nuclear wave function and an electronic factor with a parametric dependence on the nuclear configuration. Coupled equations drive

the dynamics of the two components of the wave function. In particular, a time-dependent Schrödinger equation (TDSE) describes the evolution of the nuclear wave function where the effect of the electrons, beyond BO, is accounted for in a *single*, time-dependent, potential. Compared to a formulation in terms of multiple static adiabatic (or BO) potential energy surfaces (PESs), the advantage of this formulation is evident: when the classical approximation is introduced, the force driving the nuclear evolution can be *uniquely* determined from the gradient of this time-dependent potential. [12]

In previous work we have: (i) analyzed the features of the time-dependent potential [13] in the context of non-adiabatic proton-coupled-electron-transfer, in order to pinpoint the properties that need to be accounted for when introducing approximations; (ii) determined the suitability of the classical and quasi-classical treatment [14] of nuclear dynamics, in a situation where the electronic effect can be taken into account exactly; (iii) derived an independent-trajectory (IT) mixed quantum-classical (MQC) algorithm [7, 8] to solve the coupled electronic and nuclear equations (from the factorization) in a fully approximate way. In particular, the IT-MQC scheme has been obtained as the *lowest-order* approximation, in an expansion in powers of  $\hbar$  of the nuclear wave function in the complex-phase representation. Further investigation [15] has shown, however, that corrections are required if the nuclei exhibit a quantum behavior related to a non-adiabatic event, e.g. the splitting of a nuclear wave packet after the passage through an avoided crossing.

The aim of this Letter is to go beyond the IT-MQC algorithm of Ref. [7, 8]. We have derived a coupled-trajectory (CT) MQC algorithm able to reproduce the features of the time-dependent potential, by evolving an

ensemble of classical trajectories to mimic the quantum evolution of the nuclei. Electronic populations, decoherence and spatial splitting of the nuclear wave packet are correctly reproduced when the new scheme is employed, as will be demonstrated below.

The exact factorization approach consists in writing the solution,  $\Psi(\underline{\mathbf{r}}, \underline{\mathbf{R}}, t)$ , of the TDSE  $\hat{H}\Psi = i\hbar\partial_t\Psi$ , as the single product  $\Psi(\underline{\mathbf{r}}, \underline{\mathbf{R}}, t) = \Phi_{\underline{\mathbf{R}}}(\underline{\mathbf{r}}, t)\chi(\underline{\mathbf{R}}, t)$ , where  $\Phi_{\underline{\mathbf{R}}}(\underline{\mathbf{r}}, t)$  is an electronic factor parametrically depending on the nuclear positions and  $\chi(\underline{\mathbf{R}}, t)$  is a nuclear wave function. Here,  $\hat{H} = \hat{T}_n + \hat{H}_{BO}$  is the Hamiltonian describing the system of interacting electrons and nuclei, with  $\hat{T}_n$  the nuclear kinetic energy and  $\hat{H}_{BO}$  the BO Hamiltonian containing all interactions among the particles and the electronic kinetic energy. The positions of  $N_e$  electrons and  $N_n$  nuclei are represented by the symbols  $\underline{\mathbf{r}}$  and  $\underline{\mathbf{R}}$ , respectively. The product-form of  $\Psi$  is unique, up to within an  $(\underline{\mathbf{R}}, t)$ -dependent gauge-like transformation, if the partial normalization condition,  $\int d\underline{\mathbf{r}}|\Phi_{\underline{\mathbf{R}}}(\underline{\mathbf{r}}, t)|^2 = 1 \forall \underline{\mathbf{R}}, t$ , is imposed. The evolution of the two components of the full wave function is governed by an electronic equation,

$$\left[\hat{H}_{BO} + \hat{U}_{en}[\Phi_{\underline{\mathbf{R}}}, \chi] - \epsilon(\underline{\mathbf{R}}, t)\right]\Phi_{\underline{\mathbf{R}}} = i\hbar\partial_t\Phi_{\underline{\mathbf{R}}}, \quad (1)$$

and a nuclear equation,

$$\left[\sum_{\nu=1}^{N_n} \frac{[-i\hbar\nabla_{\nu} + \mathbf{A}_{\nu}(\underline{\mathbf{R}}, t)]^2}{2M_{\nu}} + \epsilon(\underline{\mathbf{R}}, t)\right]\chi = i\hbar\partial_t\chi, \quad (2)$$

which are exactly equivalent to the full TDSE. The electron-nuclear coupling operator,

$$\begin{aligned} \hat{U}_{en}[\Phi_{\underline{\mathbf{R}}}, \chi] &= \sum_{\nu=1}^{N_n} \frac{[-i\hbar\nabla_{\nu} - \mathbf{A}_{\nu}(\underline{\mathbf{R}}, t)]^2}{2M_{\nu}} \\ &+ \frac{1}{M_{\nu}} \left( \frac{-i\hbar\nabla_{\nu}\chi}{\chi} + \mathbf{A}_{\nu}(\underline{\mathbf{R}}, t) \right) \left( -i\hbar\nabla_{\nu} - \mathbf{A}_{\nu}(\underline{\mathbf{R}}, t) \right), \end{aligned} \quad (3)$$

represents the effect of the nuclei on electronic dynamics; in turn, the time-dependent vector potential,

$$\mathbf{A}_{\nu}(\underline{\mathbf{R}}, t) = \langle \Phi_{\underline{\mathbf{R}}}(t) | -i\hbar\nabla_{\nu} \Phi_{\underline{\mathbf{R}}}(t) \rangle_{\underline{\mathbf{r}}}, \quad (4)$$

and time-dependent PES (TDPES),

$$\epsilon(\underline{\mathbf{R}}, t) = \langle \Phi_{\underline{\mathbf{R}}}(t) | \hat{H}_{BO} + \hat{U}_{en} - i\hbar\partial_t | \Phi_{\underline{\mathbf{R}}}(t) \rangle_{\underline{\mathbf{r}}}, \quad (5)$$

account for the electronic back-reaction on the nuclei in a Schrödinger-like equation. These potentials are uniquely determined [11] up to within a gauge transformation.

The CT-MQC scheme adopts a description of nuclear dynamics in terms of classical trajectories,  $\underline{\mathbf{R}}^{(I)}(t)$ , thus all quantities depending on  $\underline{\mathbf{R}}, t$  will become functions

of  $\underline{\mathbf{R}}^{(I)}(t), t$ . Nuclear dynamics will be *sampled* using trajectories, meaning that we track the evolution of a nuclear wave packet by looking at how the trajectories evolve in time. Information about the nuclear space  $\underline{\mathbf{R}}$  is only available at the instantaneous positions along the classical paths. It follows that we will not be able to calculate partial time derivatives, but only total time derivatives, by using the chain rule  $d/dt = \partial_t + \sum_{\nu} \mathbf{V}_{\nu}^{(I)} \cdot \nabla_{\nu}$ , with  $\mathbf{V}_{\nu}^{(I)} = \dot{\underline{\mathbf{R}}}_{\nu}^{(I)}(t)$  the nuclear velocity. Henceforth, the superscript  $(I)$  will be used to indicate a spatial dependence, e.g.,  $\mathbf{A}_{\nu}^{(I)}(t) = \mathbf{A}_{\nu}(\underline{\mathbf{R}}^{(I)}(t), t)$ .

The main steps in the derivation of the new CT-MQC scheme are the following: (a) we approximate the TD-PES, to avoid expensive calculations of second-order derivatives of the electronic wave function with-respect to the nuclear coordinates; (b) we fix the gauge freedom; (c) we introduce a quasi-classical interpretation of the nuclear wave function, whose phase is connected to the classical momentum and modulus reconstructed in terms of Gaussian wave packets; (d) we expand the electronic wave function on the adiabatic basis (Born-Huang expansion),  $\Phi^{(I)}(t) = \sum_l |C_l^{(I)}(t)| \exp[(i/\hbar)\gamma_l^{(I)}(t)] \varphi_l^{(I)}$ , hence a set of partial differential equations for the coefficients of the expansion will be coupled to the nuclear equation. Also the full wave function can be expanded on the adiabatic basis, with coefficients  $F_l(\underline{\mathbf{R}}, t)$ , for the exact expression, or  $F_l^{(I)}(t)$ , for the quantum-classical case, and will be referred to as BO-projected wave packets.

(a) In the expression of the TDPES we neglect the contribution of  $\langle \Phi_{\underline{\mathbf{R}}}(t) | \hat{U}_{en} | \Phi_{\underline{\mathbf{R}}}(t) \rangle_{\underline{\mathbf{r}}}$ . Notice that the expectation value on  $\Phi_{\underline{\mathbf{R}}}$  of the second line of Eq. (3) is zero by construction, thus the neglected term in the expression of the TDPES contains the second-order variations of the electronic state with-respect to the nuclear coordinates, which is small [16–18] compared to the first-order. Therefore, the TDPES is approximated as  $\epsilon(\underline{\mathbf{R}}, t) \simeq \epsilon_0(\underline{\mathbf{R}}, t) + \epsilon_{TD}(\underline{\mathbf{R}}, t)$  and Eqs. (1) and (2) become

$$i\hbar\dot{\Phi}^{(I)} = \hat{H}_{BO}\Phi^{(I)} - \sum_{\nu=1}^{N_n} \frac{\mathcal{P}_{\nu}^{(I)}}{M_{\nu}} \cdot (\mathbf{A}_{\nu}^{(I)} + i\hbar\nabla_{\nu}) \Phi^{(I)} \quad (6)$$

and

$$\begin{aligned} \mathbf{F}_{\nu}^{(I)} &= - \left\langle \Phi^{(I)} \left| \left( \nabla_{\nu} \hat{H}_{BO} \right) \right| \Phi^{(I)} \right\rangle_{\underline{\mathbf{r}}} \\ &+ \sum_{\nu'=1}^{N_n} \frac{2i\mathcal{P}_{\nu'}^{(I)}}{\hbar M_{\nu'}} \left( \mathbf{A}_{\nu'}^{(I)} \mathbf{A}_{\nu}^{(I)} - \hbar^2 \Re \left\langle \nabla_{\nu'} \Phi^{(I)} \left| \nabla_{\nu} \Phi^{(I)} \right\rangle_{\underline{\mathbf{r}}} \right), \end{aligned} \quad (7)$$

respectively, where the symbol  $\dot{\Phi}^{(I)}$  is used to indicate the full time-derivative of the electronic wave function and  $\mathcal{P}_{\nu}^{(I)}$  will be specified below. The equations have been cast in such a way that the first terms on the

right-hand-side are exactly the same as in the Ehrenfest scheme [19]. The additional terms are corrections, whose effect will be now investigated.

(b) In deriving these expressions for the evolution of the electronic wave function, Eq. (6), and for the classical nuclear force, Eq. (7), the gauge freedom has been fixed by imposing  $\epsilon_0^{(I)}(t) + \epsilon_{\text{TD}}^{(I)}(t) + \sum_{\nu} \mathbf{V}_{\nu}^{(I)} \cdot \mathbf{A}_{\nu}^{(I)}(t) = 0$ .

(c) The corrections beyond-Ehrenfest in Eqs. (6) and (7) contain a term  $\mathcal{P}_{\nu}^{(I)}(t) = -i\hbar \nabla_{\nu} |\chi^{(I)}(t)| / |\chi^{(I)}(t)|$ , which we will refer to as *quantum momentum*. The reason for this choice lies in the following expression

$$\frac{-i\hbar \nabla_{\nu} \chi(\underline{\mathbf{R}}, t)}{\chi(\underline{\mathbf{R}}, t)} + \mathbf{A}_{\nu}(\underline{\mathbf{R}}, t) \simeq \mathbf{P}_{\nu}^{(I)}(t) + \mathcal{P}_{\nu}^{(I)}(t) \quad (8)$$

for the term in Eq. (3) that explicitly depends on the nuclear wave function. Such term has to be approximated when a trajectory-based treatment is adopted. In fact, Eq. (8) has been obtained by writing the nuclear wave function in polar form,  $\chi = |\chi|e^{iS/\hbar}$ , and then identifying (quasi-classically)  $\nabla_{\nu} S + \mathbf{A}_{\nu} = \mathbf{P}_{\nu}$ , with  $\mathbf{P}_{\nu}$  the classical nuclear momentum and  $\dot{\mathbf{P}}_{\nu} = \mathbf{F}_{\nu}$  from Eq. (7).

(d) If compared to the Ehrenfest scheme, the implementation of the CT-MQC algorithm based on Eqs. (6) and (7) requires only two additional steps: the calculation of (i)  $\nabla_{\nu} \Phi^{(I)}$  and (ii)  $\mathcal{P}_{\nu}^{(I)}$ . We employ the Born-Huang expansion of  $\Phi^{(I)}$ , in order to express the term (i) using the derivatives of the expansion coefficients, indicated by the symbols  $C_i^{(I)}(t)$ , and the non-adiabatic coupling vectors. The approximation  $\nabla_{\nu} C_i^{(I)} \simeq (i/\hbar) \nabla_{\nu} \gamma_l^{(I)} C_i^{(I)}$  used here, with  $\gamma_l^{(I)}(t)$  the phase of  $C_i^{(I)}(t)$ , is consistent with previous analysis reported in Refs. [13, 14]. Moreover, based on quasi-classical considerations described in detail in the Supplemental Material, we further approximate  $\nabla_{\nu} \gamma_l^{(I)}(t) \simeq -\int^t d\tau \nabla_{\nu} \epsilon_{BO}^{(l),(I)}$ . The term (ii) is calculated assuming that the nuclear density is a combination of Gaussian-shaped wave packets, each corresponding to a given adiabatic state. Notice that this approximation is not used in general in the algorithm, but only to estimate the quantum momentum. For a two-state model,  $\mathcal{P}_{\nu}^{(I)}$  becomes [15] a linear function in the region where  $\rho_l^{(I)}(t) = |C_l^{(I)}(t)|^2 \neq 0, 1$ , while it is set to zero elsewhere (see the Supplemental Material and the discussion below). The generalization of this approximation to multiple states is straightforward and will be presented elsewhere [20]. The parameters of such linear function are the slope and the  $y$ -intercept, where the former is determined analytically by using Gaussian-shaped nuclear wave packets and the latter is obtained by enforcing (the reasonably physical condition) that no population exchange occurs when the non-adiabatic coupling vectors are zero. Information about the positions of all trajectories at a given time is required when evaluating these

two parameters, thus resulting in a procedure beyond the IT-MQC approach: the classical trajectories cannot be evolved independently from each other, they are *coupled*.

The major advantage of the CT-MQC scheme developed here is that this procedure naturally incorporates *decoherence* effects. In the following we shall discuss this feature in detail. After the nuclear wave packet has left a region of strong non-adiabatic coupling, the population  $\rho_l^{(I)}(t) = |C_l^{(I)}(t)|^2$  of the  $l$ -th BO state changes in time as

$$\dot{\rho}_l^{(I)} = - \sum_{\nu=1}^{N_n} \frac{2i\mathcal{P}_{\nu}^{(I)}}{\hbar M_{\nu}} \cdot \left( \mathbf{A}_{\nu}^{(I)} - \nabla_{\nu} \gamma_l^{(I)} \right) \rho_l^{(I)}. \quad (9)$$

In this region, the expression of the vector potential reduces to  $\mathbf{A}_{\nu}^{(I)}(t) = \sum_l \rho_l^{(I)}(t) \nabla_{\nu} \gamma_l^{(I)}(t)$ , since the non-adiabatic coupling vectors are negligible. In Eq. (9) we observe that, once  $\rho_l^{(I)}(t)$  has approached the values 0 or 1, the term on the right-hand-side becomes zero, thus the electronic population remains constant (to 0 or 1)  $\forall l$ . This is a clear indication of *decoherence*, since the (squared-modulus of the) off-diagonal elements of the electronic density matrix, often used as a measure of electronic coherence, become zero. Therefore, the correction terms beyond-Ehrenfest in Eqs. (6) and (7), proportional to the quantum momentum, will be referred to as *decoherence terms*. Obtaining this feature is a clear improvement over the Ehrenfest approach and, likewise, over the IT-MQC approach [7, 8] deduced from the exact factorization. Decoherence naturally appears by including dominant corrections in the expression of the nuclear wave function, leading to the appearance of the quantum momentum.

Numerical results obtained by implementing the above-described method are shown below in comparison to exact calculations. We discuss the performance of the CT-MQC algorithm in comparison to Ehrenfest dynamics for a two-state problem [21] involving the passage of the nuclear wave packet through a single avoided crossing, case (1), and in comparison to trajectory surface hopping (TSH) for a two-state problem involving the reflection of the nuclear wave packet from a potential barrier and its consequent spatial splitting, case (2), commonly known as Tully-3 model [9]. The computational details for these two problems are given in the Supplemental Material.

The TDPEs for model case (1) is shown in Fig. 1 (upper panels). It develops steps and the nuclear wave packet correctly splits at the avoided crossing (Fig. 1, lower panels). It is worth noting that Ehrenfest dynamics completely misses the splitting, as we have shown in Ref. [8]. Furthermore, despite the fact that Ehrenfest dynamics properly reproduces the populations of the electronic states, as shown in Fig. 3 (upper left panel), it does not capture decoherence. On the contrary, the

CT-MQC procedure slightly underestimates the non-adiabatic population exchange but correctly reproduce decoherence (Fig. 3, lower left panel).

In Fig. 3, we have used the quantity  $N_{traj}^{-1} \sum_I \rho_1^{(I)}(t) \rho_2^{(I)}(t)$  as measure of decoherence, whose quantum equivalent is  $\int d\mathbf{R} \rho_1(\mathbf{R}, t) \rho_2(\mathbf{R}, t) |\chi(\mathbf{R}, t)|^2$ . Here, the nuclear density has been replaced by its “classical” approximation, i.e.  $|\chi(\mathbf{R}, t)|^2 \simeq N_{traj}^{-1} \sum_I \delta(\mathbf{R} - \mathbf{R}^{(I)}(t))$ .

We show in Fig. 2 (lower panels) that the CT-MQC algorithm reproduces the splitting of the nuclear wave packet due to the reflection from the barrier. In fact, the TD PES develops the well-studied [13] steps (Fig. 2, upper panels) that bridge piecewise adiabatic shapes and allow trajectories in different regions of space to feel different forces. This feature is the strength of a procedure based on the exact factorization: a *single* time-dependent potential generating very different forces in different regions of space. It is known [9] that TSH as well is able to capture the reflection event for a low initial momentum of the nuclear wave packet, but suffers from over-coherence [10, 22]. In fact, as shown in Fig. 3, TSH completely misses decoherence, whereas the CT-MQC scheme not only reproduces the populations of the electronic states as functions of time (Fig. 3, upper right panel), but can also capture electronic decoherence (Fig. 3, lower right panel). The comparison between exact and CT-MQC results is overall remarkable and a clear step forward in comparison to other methods.

In this Letter we have proposed a CT-MQC scheme based on the exact factorization formalism and tested it on a typical example of electronic non-adiabatic process. The resulting equations give additional terms compared to Ehrenfest dynamics, that appear to be responsible for decoherence. The comparison of the CT-MQC scheme with full quantum mechanical results shows that we can correctly predict both electronic and nuclear properties: population dynamics, nuclear wave packet splitting and decoherence. Non-adiabatic transitions are induced by the classical nuclear momentum, the zero-th order term of the  $\hbar$ -expansion of the nuclear wave function, and decoherence is the effect of the dominant corrections to the momentum. In addition, we have proven that, as discussed in our previous work [13, 14], being able to catch the main features of the time-dependent potential in an approximate scheme results in the correct description of the nuclear dynamics. The major advantages of our CT-MQC algorithm over commonly used methods are: (1) the working equations are conceptually and computationally as simple as Ehrenfest equations, and (2) a small number of trajectories is required, because *only* initial conditions are to be sampled (no stochastic element is introduced). Working in the framework of the exact factorization allows to systematically improve previous approximations, as we have shown in this Letter in com-

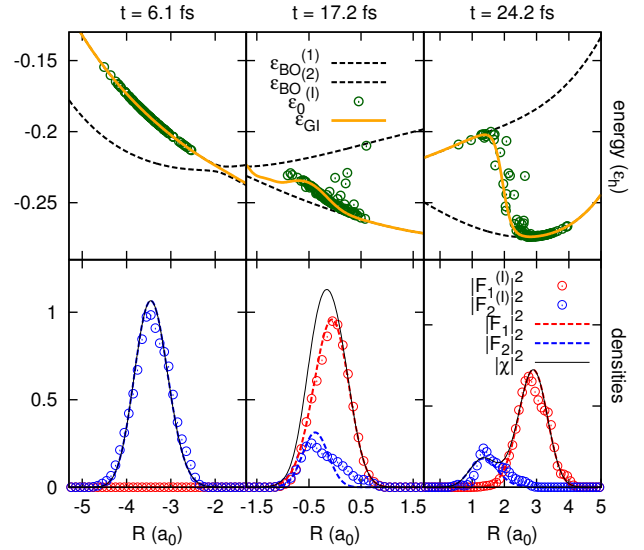


FIG. 1. Snapshots at different times for model case (1) of: (top) the gauge-invariant (GI) part of the scalar potential  $\epsilon_{GI}(\mathbf{R}, t) = \langle \Phi_{\mathbf{R}}(t) | \hat{H}_{BO} + \hat{U}_{en} | \Phi_{\mathbf{R}}(t) \rangle_{\mathbf{E}}$  (lines) compared to its approximation  $\epsilon_0^{(I)}(t)$  (dots) used in the CT-MQC calculations, in Hartree  $\epsilon_h$  (the BO surface are plotted for reference as dashed black lines); (bottom) nuclear density  $|\chi(\mathbf{R}, t)|^2$  (black line) and BO-projected densities (dashed lines) compared to the values of the BO-projected densities along the trajectories (dots).

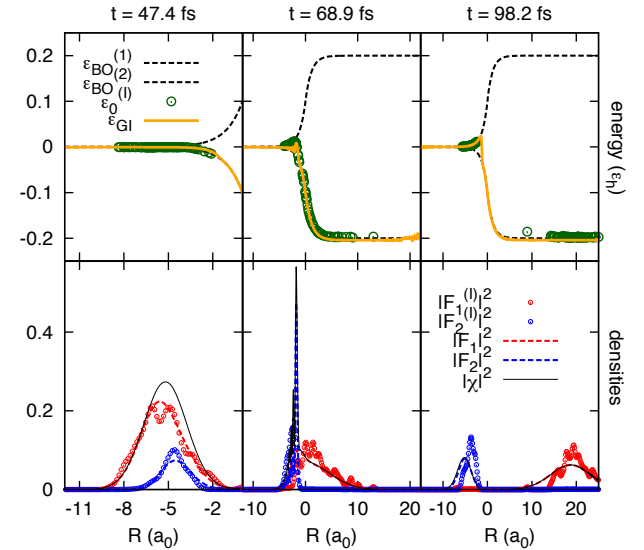


FIG. 2. Same as Fig. 1 for model case (2).

parison to the IT-MQC of Ref. [7, 8]. Along similar lines, future work will focus on including quantum nuclear effects, such as interference, adopting a semiclassical representation of nuclear dynamics.

Partial support from the Deutsche Forschungsgemeinschaft (SFB 762) and from the European Commis-

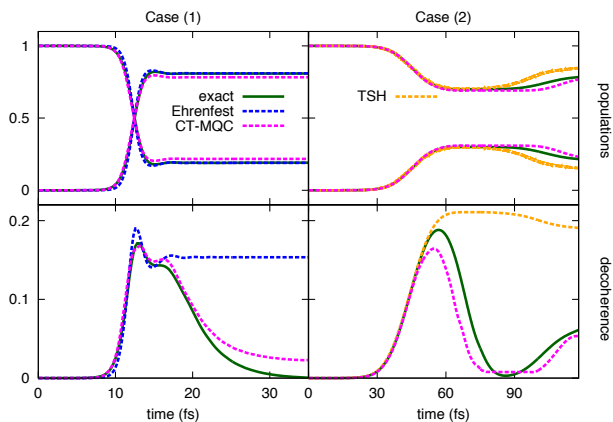


FIG. 3. Populations of the BO states (upper panels) and indicator of decoherence (lower panels) as functions of time for model case (1) (left) and model case (2) (right).

sion (FP7-NMP-CRONOS) is gratefully acknowledged.

- [1] D. Polli, P. Altoè, O. Weingart, K. M. Spillane, C. Manzoni, D. Brida, G. Tomasello, G. Orlandi, P. Kukura, R. A. Mathies, M. Garavelli, and G. Cerullo, *Nature* **467**, 440 (2010); S. Hayashi, E. Tajkhorshid, and K. Schulten, *Biophys. J.* **416**, 403 (2009); W. C. Chung, S. Nanbu, and T. Ishida, *J. Phys. Chem. B* **116**, 8009 (2012).
- [2] E. Tapavicza, A. M. Meyer, and F. Furche, *Phys. Chem. Chem. Phys.* **13**, 20986 (2011); T. Brixner, J. Stenger, H. M. Vaswani, M. Cho, R. E. Blankenship, and G. R. Fleming, *Nature* **434**, 625 (2005).
- [3] C. A. Rozzi, S. M. Falke, N. Spallanzani, A. Rubio, E. Molinari, D. Brida, M. Maiuri, G. Cerullo, H. Schramm, J. Christoffers, and C. Lienau, *Nat. Commun.* **4**, 1602 (2013); C. Silva, *Nat. Mater.* **12**, 5 (2013); A. E. Jailaubekov, A. P. Willard, J. R. Tritsch, W.-L. Chan, N. Sai, R. Gearba, L. G. Kaake, K. J. Williams, K. Leung, P. J. Rossky, and X.-Y. Zhu, *ibid.* **12**, 66 (2013).
- [4] A. L. Sobolewski, W. Domcke, C. Dedonder-Lardeux, and C. Jouvet, *Phys. Chem. Chem. Phys.* **4**, 1093 (2002); M. T. do N. Varella, Y. Arasaki, H. Ushiyama, V. McKoy, and K. Takatsukas, *J. Chem. Phys.* **124**, 154302 (2006); J.-Y. Fang and S. Hammes-Schiffer, *ibid.* **107**, 8933 (1997); D. Marx, *Chem. Phys. Chem.* **7**, 1848 (2006).
- [5] T. J. Martínez and R. D. Levine, *Chem. Phys. Lett.* **259**, 252 (1996); T. J. Martínez, M. Ben-Nun, and R. D. Levine, *J. Phys. Chem.* **100**, 7884 (1996); T. J. Martínez, *Acc. Chem. Res.* **39**, 119 (2006); H.-D. Meyer, U. Manthe, and L. S. Cederbaum, *Chem. Phys. Lett.* **165**, 73 (1990); I. Burghardt, H.-D. Meyer, and L. S. Cederbaum, *J. Chem. Phys.* **111**, 2927 (1999); H.-D. Meyer and G. A. Worth, *Theor. Chim. Acta* **109**, 251 (2003); M. Thoss, W. Domcke, and H. Wang, *Chem. Phys.* **296**, 217 (2004); H. Wang and M. Thoss, *J. Chem. Phys.* **119**, 1289 (2003); J. Li, I. Kondov, H. Wang, and M. Thoss, *J. Phys. Chem. C* **114**, 18481 (2010); Q. Meng, S. Faraji, O. Vendrell, and H.-D. Meyer, *J. Chem. Phys.* **137**, 134302 (2012); M. Schröder, J.-L. Carreón-Macedo, and A. Brown, *Phys. Chem. Chem. Phys.* **10**, 850 (2008).
- [6] P. Ehrenfest, *Zeitschrift für Physik* **45**, 455 (1927); D. V. Shalashilin, *J. Chem. Phys.* **130**, 244101 (2009); R. Kapral and G. Ciccotti, *J. Chem. Phys.* **110**, 8916 (1999); B. F. E. Curchod, I. Tavernelli, and U. Rothlisberger, *Phys. Chem. Chem. Phys.* **13**, 3231 (2011); S. Bonella and D. F. Coker, *J. Chem. Phys.* **122**, 194102 (2005); N. L. Doltsinis and D. Marx, *Phys. Rev. Lett.* **88**, 166402 (2002); P. Pechukas, *Phys. Rev.* **181**, 166 (1969); J. E. Subotnik, *J. Chem. Phys.* **132**, 134112 (2010); Y. Wu and M. Herman, *ibid.* **123**, 1 (2005); D. F. Coker and L. Xiao, *ibid.* **102**, 496 (1995); O. V. Prezhdo and P. J. Rossky, *ibid.* **107**, 825 (1997); G. Stock and M. Thoss, *Phys. Rev. Lett.* **78**, 578 (1997); X. Sun and W. H. Miller, *J. Chem. Phys.* **106**, 6346 (1997); A. W. Jasper, C. Zhu, S. Nangia, and D. G. Truhlar, *Faraday Discuss.* **127**, 1 (2004); S. Nielsen, R. Kapral, and G. Ciccotti, *J. Chem. Phys.* **112**, 6543 (2000); C.-Y. Hsieh and R. Kapral, *ibid.* **138**, 134110 (2013); P. Huo and D. F. Coker, *ibid.* **137**, 22A535 (2012); R. E. Wyatt, C. L. Lopreore, and G. Parlant, *ibid.* **114**, 5113 (2001); I. Burghardt, *ibid.* **122**, 094103 (2005); O. V. Prezhdo and C. Brooksby, *Phys. Rev. Lett.* **86**, 3215 (2001); N. Zamstein and D. J. Tannor, *J. Chem. Phys.* **137**, 22A518 (2012); D. Bousquet, K. H. Hughes, D. A. Micha, and I. Burghardt, *ibid.* **134**, 064116 (2011); J. O. Richardson and M. Thoss, *ibid.* **139**, 031102 (2013); N. Ananth, *ibid.* **139**, 124102 (2013); F. Agostini, S. Caprara, and G. Ciccotti, *Europhys. Lett.* **78**, 30001 (2007).
- [7] A. Abedi, F. Agostini, and E. K. U. Gross, *Europhys. Lett.* **106**, 33001 (2014).
- [8] F. Agostini, A. Abedi, and E. K. U. Gross, *J. Chem. Phys.* **141**, 214101 (2014).
- [9] J. C. Tully, *J. Chem. Phys.* **93**, 1061 (1990).
- [10] J. E. Subotnik and N. Shenvi, *J. Chem. Phys.* **134**, 244114 (2011); B. R. Landry and J. E. Subotnik, *ibid.* **135**, 191101 (2011); J. E. Subotnik and N. Shenvi, *ibid.* **134**, 024105 (2011); J. E. Subotnik, N. Shenvi, and W. Yang, *ibid.* **135**, 024101 (2011); B. F. E. Curchod and I. Tavernelli, *ibid.* **138**, 184112 (2013); T. J. Penfold and G. A. Worth, *J. Mol. Graph. and Mod.* **26**, 613 (2007); G. A. Worth, P. Hunt, and M. A. Robb, *J. Chem. Phys. A* **26**, 613 (2003); D. Kohen, F. H. Stillinger, and J. C. Tully, *J. Chem. Phys.* **109**, 4713 (1998).
- [11] A. Abedi, N. T. Maitra, and E. K. U. Gross, *Phys. Rev. Lett.* **105**, 123002 (2010); *J. Chem. Phys.* **137**, 22A530 (2012).
- [12] It should be noted that in addition to the scalar potential energy surface there is, in the most general case, also a Berry-type vector potential, as is evident in Eqs. (2-4). In some cases this vector potential may vanish identically (see [S. K. Min, A. Abedi, K. S. Kim and E. K. U. Gross, *Phys. Rev. Lett.* **113** 263004 (2014)]).
- [13] A. Abedi, F. Agostini, Y. Suzuki, and E. K. U. Gross, *Phys. Rev. Lett.* **110**, 263001 (2013).
- [14] F. Agostini, A. Abedi, Y. Suzuki, and E. K. U. Gross, *Mol. Phys.* **111**, 3625 (2013); F. Agostini, A. Abedi, Y. Suzuki, S. K. Min, N. T. Maitra, and E. K. U. Gross, *J. Chem. Phys.* **142**, 084303 (2015).
- [15] F. Agostini, S. K. Min, and E. K. U. Gross, *Ann. Phys.*, Doi: 10.1002/andp.201500108 (2015).
- [16] N. C. Handy, Y. Yamaguchi, and H. F. Schaefer III, *J. Chem. Phys.* **84**, 4481 (1986).
- [17] E. F. Valeev and C. D. Sherrill, *J. Chem. Phys.* **118**, 3921 (2003).

- [18] We note that  $\Phi_{\underline{\mathbf{R}}}(\underline{\mathbf{r}}, t)$  may contain a translational phase like  $e^{i\underline{\mathbf{K}} \cdot \underline{\mathbf{R}}}$  where  $\underline{\mathbf{K}}$  is the linear momentum associated to the motion of the nuclear system as a rigid body. The second derivative with respect to  $\underline{\mathbf{R}}_i$  then yields a term proportional to  $\underline{\mathbf{K}}_i^2$  which is proportional to  $M_i^2$ . However, the vector potential in the neglected term of the TDPES contains a similar term which cancels out all  $M_i^2$  dependencies.
- [19] J. C. Tully, in *Classical and quantum dynamics in condensed phase simulations*, Proceedings of the international school of physics, edited by B. B. Berne, G. Cicciotti, and D. F. Coker (1997).
- [20] S. K. Min, F. Agostini, and E. K. U. Gross, to be submitted.
- [21] S. Shin and H. Metiu, *J. Chem. Phys.* **102**, 23 (1995).
- [22] J. E. Subotnik, W. Ouyang, and B. R. Landry, *J. Chem. Phys.* **139**, 214107 (2013).

# Supplemental Material to “A coupled-trajectory quantum-classical approach to electronic decoherence in non-adiabatic processes”

Seung Kyu Min,<sup>1,2</sup> Federica Agostini,<sup>1</sup> and E. K. U. Gross<sup>1</sup>

<sup>1</sup>*Max-Planck Institut für Mikrostrukturphysik,  
Weinberg 2, D-06120 Halle, Germany*

<sup>2</sup>*Department of Chemistry, School of Natural Science,  
Ulsan National Institute of Science and Technology (UNIST), Ulsan 689-798, Korea*

(Dated: October 12, 2018)

arXiv:1504.00250v2 [physics.chem-ph] 27 Jun 2015

In the Letter we state that the main evolution equations of the coupled-trajectory mixed quantum-classical (CT-MQC) scheme can be cast such that corrections terms to Ehrenfest-like equations arise naturally when the *quantum momentum* is included. Here, we will present this result by employing the Born-Huang expansion to represent the electronic wave function  $\Phi_{\underline{\mathbf{R}}}(\underline{\mathbf{r}}, t)$  as a superposition of adiabatic states. Alternative expressions of Eqs. (6) and (7) of the Letter will be derived. Notice that this operation is simply a way to re-write Eqs. (6) and (7), no additional approximations are considered, rather than those already discussed in the Letter.

## EQUATIONS EMPLOYING THE BORN-HUANG EXPANSION

The adiabatic states are the eigenvectors of the Born-Oppenheimer (BO) Hamiltonian,  $\hat{H}_{BO}$ , and are indicated by the symbols  $\{\varphi_{\underline{\mathbf{R}}}^{(l)}(\underline{\mathbf{r}})\}_{l=1, N_{st}}$ , where  $N_{st}$  is the number of states that will be included in the expansion. The corresponding eigenvalues are labeled as  $\epsilon_{BO}^{(l)}(\underline{\mathbf{R}})$ . The Born-Huang expansion is

$$\Phi_{\underline{\mathbf{R}}}(\underline{\mathbf{r}}, t) = \sum_{l=1}^{N_{st}} |C_l(\underline{\mathbf{R}}, t)| \exp\left[\frac{i}{\hbar}\gamma_l(\underline{\mathbf{R}}, t)\right] \varphi_{\underline{\mathbf{R}}}^{(l)}(\underline{\mathbf{r}}), \quad (\text{SM.1})$$

where the coefficients  $C_l(\underline{\mathbf{R}}, t)$  have been written in terms of their moduli,  $|C_l(\underline{\mathbf{R}}, t)|$ , and phases,  $\gamma_l(\underline{\mathbf{R}}, t)$ .

The evolution equations for the coefficients  $C_l(\underline{\mathbf{R}}, t)$  and the classical nuclear force, from Eqs. (6) and (7), can be written now as

$$\dot{C}_l^{(I)}(t) = \frac{-i}{\hbar} \epsilon_{BO}^{(l), (I)} C_l^{(I)}(t) - \sum_{\nu=1}^{N_n} \mathbf{v}^{(I)}(t) \cdot \sum_{k=1}^{N_{st}} C_k^{(I)}(t) \mathbf{d}_{\nu, lk}^{(I)} \quad (\text{SM.2})$$

$$+ \sum_{\nu=1}^{N_n} \frac{1}{M_\nu} \frac{\nabla_\nu |\chi^{(I)}(t)|}{|\chi^{(I)}(t)|} \cdot \left( \mathbf{A}_\nu^{(I)}(t) - \mathbf{f}_{\nu, l}^{(I)}(t) \right) C_l^{(I)}(t) \quad (\text{SM.3})$$

and

$$\mathbf{F}_\nu^{(I)}(t) = - \sum_{l=1}^{N_{st}} \rho_l^{(I)}(t) \nabla_\nu \epsilon_{BO}^{(l), (I)} - \sum_{k>l,=1}^{N_{st}} 2\Re \left[ \rho_{lk}^{(I)}(t) \right] \left( \epsilon_{BO}^{(k), (I)} - \epsilon_{BO}^{(l), (I)} \right) \mathbf{d}_{\nu, lk}^{(I)} \quad (\text{SM.4})$$

$$+ \sum_{\nu'=1}^{N_{st}} \frac{2}{M_{\nu'}} \frac{\nabla_{\nu'} |\chi^{(I)}(t)|}{|\chi^{(I)}(t)|} \cdot \mathcal{F}_{\nu'\nu}^{(I)}(t), \quad (\text{SM.5})$$

with  $\nabla_\nu |\chi^{(I)}(t)|/|\chi^{(I)}(t)| = (i/\hbar)\mathcal{P}_\nu^{(I)}(t)$ . Here, in order to adopt the same notation used in the main text, we indicate the  $\underline{\mathbf{R}}$ -dependence by introducing the label  $(I)$ , the trajectory, and dropping the label  $\underline{\mathbf{R}}$ . New symbols have been introduced, namely

$$\rho_l^{(I)}(t) = \left| C_l^{(I)}(t) \right|^2 \quad \text{and} \quad \rho_{lk}^{(I)}(t) = C_l^{(I)*}(t) C_k^{(I)}(t), \quad (\text{SM.6})$$



the standard non-adiabatic coupling vectors, defined as

$$\mathbf{d}_{\nu,lk}^{(I)} = \langle \varphi^{(l),(I)} | \nabla_{\nu} \varphi^{(k),(I)} \rangle_{\underline{\mathbf{r}}}, \quad (\text{SM.7})$$

the gradient of the phases,  $\gamma_l^{(I)}(t)$ , of the expansion coefficients in Eq. (SM.1)

$$\mathbf{f}_{\nu,l}^{(I)}(t) = \nabla_{\nu} \gamma_l^{(I)}(t) \quad (\text{SM.8})$$

and the matrix

$$\mathcal{F}_{\nu\nu}^{(I)}(t) = \sum_{l=1}^{N_{st}} \rho_l^{(I)}(t) \mathbf{f}_{\nu,l}^{(I)}(t) \wedge \left( \mathbf{A}_{\nu}^{(I)}(t) - \mathbf{f}_{\nu,l}^{(I)}(t) \right). \quad (\text{SM.9})$$

In this last expression, the symbol  $\wedge$  stands for a tensor product. Moreover, notice that, using the Born-Huang expansion in Eq. (SM.1), also the vector potential can be (exactly) re-written as

$$\mathbf{A}_{\nu}^{(I)}(t) = \sum_{l=1}^{N_{st}} \rho_l^{(I)}(t) \mathbf{f}_{\nu,l}^{(I)}(t) + 2\hbar \sum_{k>l=1}^{N_{st}} \Im \left[ \rho_{lk}^{(I)}(t) \right] \mathbf{d}_{\nu,lk}^{(I)}, \quad (\text{SM.10})$$

where real electronic BO states have been assumed.

Eqs. (SM.2) and (SM.4) are exactly the expressions appearing in the Ehrenfest algorithm, when the Born-Huang expansion is used to represent the electronic wave function. The additional terms depend on the *quantum momentum*, defined as

$$\mathcal{P}_{\nu}^{(I)}(t) = -i\hbar \frac{\nabla_{\nu} |\chi^{(I)}(t)|}{|\chi^{(I)}(t)|} \quad (\text{SM.11})$$

in Eq. (8) of the Letter.

Eqs. (SM.2) to (SM.5) are the basic equations of the CT-MQC algorithm derived and discussed in the Letter.

## APPROXIMATION FOR THE GRADIENT OF THE EXPANSION COEFFICIENTS

The quantity  $\mathbf{f}_{\nu,l}^{(I)}(t)$  appears in the evolution equations as consequence of the following approximations. The gradient of the expansion coefficients in Eq. (SM.1), namely

$$\nabla_{\nu} C_l^{(I)}(t) = \left[ \frac{i}{\hbar} \nabla_{\nu} \gamma_l^{(I)}(t) + \frac{\nabla_{\nu} |C_l^{(I)}(t)|}{|C_l^{(I)}(t)|} \right] C_l^{(I)}(t) \quad (\text{SM.12})$$

is approximated as

$$\nabla_{\nu} C_l^{(I)}(t) \simeq \frac{i}{\hbar} C_l^{(I)}(t) \nabla_{\nu} \gamma_l^{(I)}(t), \quad (\text{SM.13})$$

since we have already observed, based on full quantum calculations [1–3], that the contribution  $\nabla_\nu \left| C_l^{(I)}(t) \right|$  is considerably different from zero only in regions where the nuclear density is small and thus where only few trajectories are expected. The error introduced this way can be systematically reduced by increasing the number of trajectories.

In the calculations, we use an approximation to the term  $\nabla_\nu \gamma_l^{(I)}(t)$  based on the following quasi-classical considerations. When the Born-Huang expansion is also employed for the full wave function  $\Psi(\underline{\mathbf{r}}, \underline{\mathbf{R}}, t)$ , namely

$$\Psi(\underline{\mathbf{r}}, \underline{\mathbf{R}}, t) = \sum_{l=1}^{N_{st}} |F_l(\underline{\mathbf{R}}, t)| \exp \left[ \frac{i}{\hbar} s_l(\underline{\mathbf{R}}, t) \right] \varphi_{\underline{\mathbf{R}}}^{(l)}(\underline{\mathbf{r}}), \quad (\text{SM.14})$$

the phases of the coefficients in Eq. (SM.1) and of the coefficients  $F_l(\underline{\mathbf{R}}, t)$  are related via the expression

$$\gamma_l^{(I)}(t) = s_l^{(I)}(t) - S^{(I)}(t). \quad (\text{SM.15})$$

Here, once again, we have replaced the spatial dependence by the dependence on the trajectory  $I$  and we have used the symbol  $S^{(I)}(t)$  to indicate the phase of the nuclear wave function, as done in the Letter. Eq. (SM.15) straightforwardly follows from the factorization. If we identify the nuclear momentum calculated along the  $I$ -th trajectory as  $\nabla_\nu S^{(I)}(t) + \mathbf{A}_\nu^{(I)}(t) = \mathbf{P}_\nu^{(I)}(t)$  and similarly  $\nabla_\nu s_l^{(I)}(t) = \mathbf{p}_\nu^{(l),(I)}(t)$  as the momentum associated to the propagation of the  $l$ -th “BO-projected” wave packet  $|F_l^{(I)}(t)|^2$  on the  $l$ -th BO adiabatic surface, we can write

$$\nabla_\nu \gamma_l^{(I)}(t) \simeq \mathbf{p}_\nu^{(l),(I)}(t) - (\mathbf{P}_\nu^{(I)}(t) - \mathbf{A}_\nu^{(I)}(t)). \quad (\text{SM.16})$$

Notice that  $|F_l^{(I)}(t)|^2$  is identified [1–3] as a “BO-projected” wave packet since from the factorization it follows that  $|\chi|^2 = \sum_l |F_l|^2$ . Taking the time-derivative of both sides of Eq. (SM.16)

$$\nabla_\nu \dot{\gamma}_l^{(I)}(t) \simeq -\nabla_\nu \epsilon_{BO}^{(l),(I)} \quad (\text{SM.17})$$

since on the right-hand-side we identify the forces associated to the motions of the “BO-projected” wave packet and of the nuclear wave function. The time-derivative of the term in parenthesis in Eq. (SM.16) is identically zero because in the chosen gauge the scalar potential is zero, thus all effects of the coupling to the electrons in the nuclear equation is contained in the vector potential. Indeed, Eq. (SM.17) is valid only in the gauge we chose to derive the CT-MQC algorithm. The expression for  $\nabla_\nu \gamma_l^{(I)}(t)$  used in our algorithm thus follows,

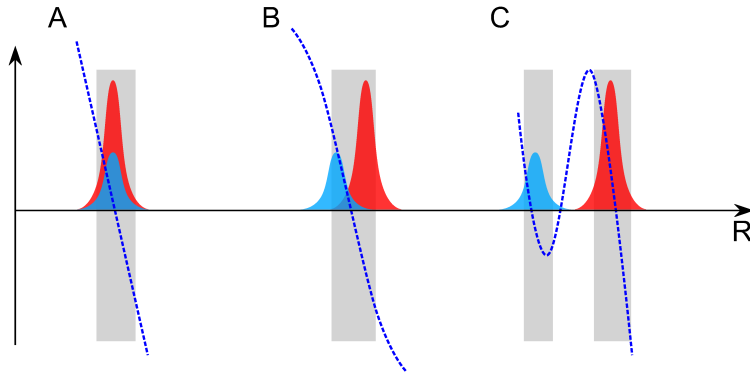
$$\mathbf{f}_{\nu,l}^{(I)}(t) = \nabla_\nu \dot{\gamma}_l^{(I)}(t) = - \int^t d\tau \nabla_\nu \epsilon_{BO}^{(l),(I)}. \quad (\text{SM.18})$$

## APPROXIMATION FOR THE QUANTUM MOMENTUM

We recall here the expression of the quantum momentum

$$\mathcal{P}_\nu^{(I)}(t) = -i\hbar \frac{\nabla_\nu |\chi^{(I)}(t)|}{|\chi^{(I)}(t)|} = -i\hbar \frac{\nabla_\nu |\chi^{(I)}(t)|^2}{2|\chi^{(I)}(t)|^2} \quad (\text{SM.19})$$

which is written in the second equality in terms of the nuclear density  $|\chi^{(I)}(t)|^2$ . In order to derive a practical way to estimate this expression, we assume that  $|\chi^{(I)}(t)|^2$  can be written as a sum of Gaussian-shaped wave packets. In the simple case of two adiabatic states, only two Gaussian functions are considered, as schematically illustrated in Fig. SM.1. We underline again (as in the Letter) that this hypothesis is introduced only to estimate the quantum momentum and not to actually solve the classical nuclear equation. We refer to [4], where we show that the approximation we use here for the quantum momentum is consistent also with a representation of the nuclear wave packet in terms of coherent states. Two scenarios may occur: (1) the BO-projected wave packets overlap



Supplemental Material, Figure SM.1. Schematic plot of the shape of the quantum momentum for various cases. The blue and red Gaussians represent BO-projected nuclear densities while the blue dashed lines are the quantum momentum (apart from the  $-i\hbar$  multiplicative factor) corresponding to each configuration of the Gaussians. The grey areas highlight the regions where the nuclear density is considerably different from zero.

and classical trajectories may be located in the overlap region; (2) the BO-projected wave packets are well-separated, thus the overlap region is poorly sampled by the trajectories since the nuclear density is small. In case (1), we use a linear function to approximate the quantum momentum, as shown in the panels (A) and (B) of Fig. SM.1, within the overlap region, while we set it equal to zero outside this region. Since outside the overlap region there is a low probability of finding trajectories, as the nuclear density is small, the final result is not strongly affected by this approximation. Moreover, as discussed in Eq. (9) in the Letter, the term in the electronic equation containing the quantum momentum vanishes outside the overlap region, if in this region the non-adiabatic coupling vectors are zero. The inverse situation occurs in case (2), where the linear approximation

does not strongly affects the trajectories, because the overlap region is poorly sampled. This is shown in the panel (C) of Fig. SM.1. Outside this region, where the majority of trajectories is located, the quantum momentum is set to zero. However, this situation in general takes place after the nuclear packet has left the region of non-adiabatic coupling, where Eq. (SM.3), containing the quantum momentum, is identically zero as discussed in the Letter in Eq. (9) (this feature is related to the fact that if  $|C_l^{(I)}(t)| = 1$  all other  $|C_k^{(I)}(t)| \forall k \neq l$  are identically zero).

## IMPLEMENTING THE CT-MQC ALGORITHM

We describe the steps necessary to implement the CT-MQC:

1. get the BO potentials  $\epsilon_{BO}^{(l),(I)}$ , along with  $\nabla_\nu \epsilon_{BO}^{(l),(I)}$ , and the non-adiabatic coupling vectors  $\mathbf{d}_{\nu,lk}^{(I)}$ ;
2. compute  $\mathbf{f}_{\nu,l}^{(I)}(t) = \nabla_\nu \gamma_l^{(I)}(t) = - \int^t d\tau \nabla_\nu \epsilon_{BO}^{(l),(I)}$ , using the BO forces;
3. collect information about the positions of all trajectories,  $\mathbf{R}^{(I)}(t)$  (this step implies that the trajectories cannot be propagated independently);
4. calculate the quantum momentum,  $\nabla_\nu |\chi^{(I)}(t)| / |\chi^{(I)}(t)| = \alpha [R^{(I)}(t) - R_M(t)]$ , where we use the symbol  $R_M(t)$  for the crossing point between the two Gaussians (the  $y$ -intercept), as illustrated in the Letter, namely by enforcing (the reasonably physical condition) that no population exchange occurs when the non-adiabatic coupling vectors are zero;
5. evolve the coefficients  $C_l^{(I)}(t)$  and the trajectories according to Eqs. (SM.2) to (SM.5);
6. go back to step 1.

## COMPUTATIONAL DETAILS

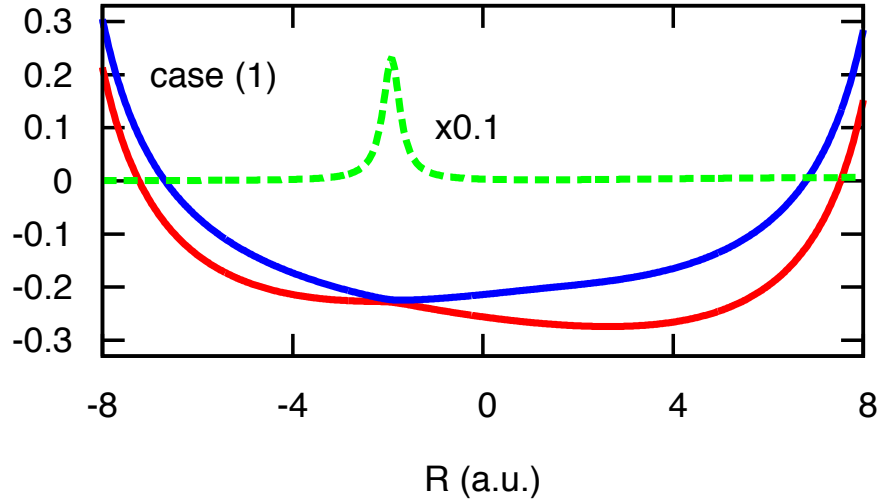
### Test case (1)

The model system for non-adiabatic charge transfer [5] analyzed in previous work [1–4, 6] has been also employed in the present study, as it exhibits the typical features of non-adiabatic processes and is exactly solvable, by integrating the full TDSE using the split-operator technique [7]. It thus provides a benchmark for the CT-MQC scheme. The system consists of three ions and one electron: two ions are fixed at a distance of  $L = 19.0 a_0$ , the third ion and the electron are free to move in one dimension along the line joining the two fixed ions. The moving ion interacts with the fixed ions via a bare Coulomb potentials, while the electron-ion interactions are treated as soft-Coulomb potentials, with parameters  $R_m = 5.0 a_0$  (moving ion),  $R_l = 3.1 a_0$  (left ion) and  $R_r = 4.0 a_0$

(right ion). The full Hamiltonian for this system is

$$\hat{H}(r, R) = -\frac{1}{2} \frac{\partial^2}{\partial r^2} - \frac{1}{2M} \frac{\partial^2}{\partial R^2} + \frac{1}{|\frac{L}{2} - R|} + \frac{1}{|\frac{L}{2} + R|} - \frac{\operatorname{erf}\left(\frac{|R-r|}{R_f}\right)}{|R-r|} - \frac{\operatorname{erf}\left(\frac{|r-\frac{L}{2}|}{R_r}\right)}{|r-\frac{L}{2}|} - \frac{\operatorname{erf}\left(\frac{|r+\frac{L}{2}|}{R_l}\right)}{|r+\frac{L}{2}|}. \quad (\text{SM.20})$$

The nuclear mass is  $M = 1836$ . With this choice of parameters the two lowest BO states are strongly coupled and there is a weak coupling to the remaining states, as shown in Fig. SM.2. The initial wave function is the product of a real-valued normalized Gaussian wave packet, centered at  $R_c = -4.0 a_0$  with variance  $\sigma = 1/\sqrt{2.85} a_0$ , and the second BO electronic state. The time-step used for integrating the TDSE is  $2.4 \times 10^{-3}$  fs (or 0.1 a.u.). CT-MQC results are obtained by propagating  $N_{\text{traj}} = 200$  trajectories whose initial positions and momenta are sampled from the Wigner distribution corresponding to the initial quantum mechanical density. In this case, the time-step is  $1.2 \times 10^{-2}$  fs (or 0.5 a.u.). The fourth-order Runge-Kutta algorithm is used to propagate the electronic equation and the velocity-Verlet algorithm is used for the nuclear equation.



Supplemental Material, Figure SM.2. Ground (red) and excited (blue) adiabatic potential energy surfaces for the model case (1). The non-adiabatic coupling between the two states is also shown (green).

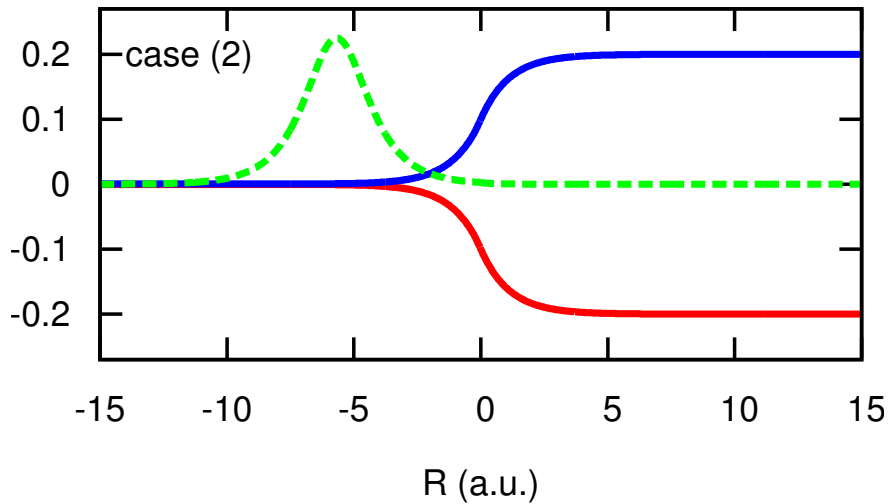
### Test case (2)

In the Letter we have reported results for the so-called Tully's model #3 [8]. It is a two-state model representing an extended coupling region with reflection. This model has been well-studied in the literature as it represents a critical test for any new approach

to non-adiabatic dynamics based on trajectories. In fact, when a nuclear wave packet starts in far negative region and moves with positive but low initial momentum, it is partially reflected by the upper surface and partially transmitted on the lower surface. This event takes place when the nuclear wave packet reaches the region of space where the two adiabatic surfaces start to significantly deviate from each other. The adiabatic potential energy surfaces are shown in Fig. SM.3, along with the non-adiabatic coupling. The analytic form [8] of the electronic Hamiltonian, in diabatic base, is

$$\begin{aligned}
 H_{11}(R) &= a, H_{22}(R) = -a, \\
 H_{12}(R) &= b \exp(cR), R < 0, \\
 H_{12}(R) &= b [2 - \exp(-cR)], R > 0, \\
 H_{21}(R) &= H_{12}(R)
 \end{aligned}
 \tag{SM.21}$$

with  $a = 6 \times 10^{-4}$ ,  $b = 0.1$ ,  $c = 0.9$ . In the Letter we show results for a low initial momentum  $\hbar k_0 = 10$  a.u., which represents a critical situation due to the high probability of the reflection channel. The initial nuclear wave packet is as Gaussian with width  $\sigma = 20/k_0$  with  $R_0 = -15.0$  a.u. the center of the Gaussian. Exact results are obtained using a wave packet propagation scheme where we chose the value 0.1 a.u. for the time-step used to integrate the TDSE. CT-MQC results are obtained by propagating a set of  $N_{traj} = 200$  trajectories whose initial positions and momenta are sampled from the Wigner distribution corresponding to the initial quantum mechanical density. The time-step is 0.5 a.u. for the CT-MQC algorithm.

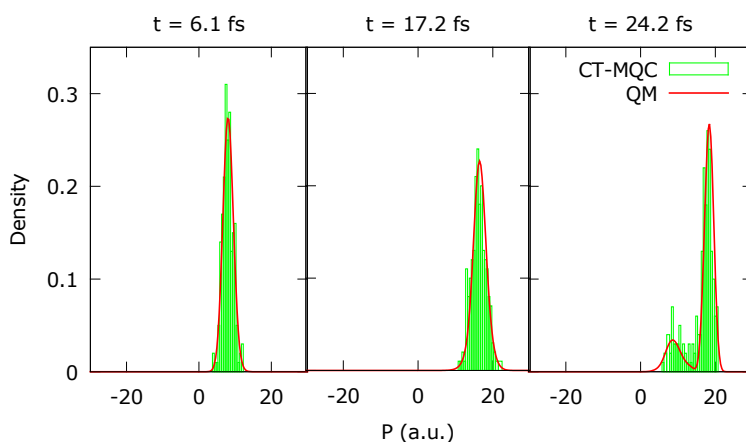


Supplemental Material, Figure SM.3. Same as in Fig. SM.2 but the model case (2).

### Analysis in momentum space

We have observed in the Letter that decoherence starts manifesting itself when the nuclear density splits in configuration space. The two events, in fact, are strongly related:

decoherence cannot be appropriately reproduced if the wave packets propagates “coherently”, without splitting. However, the deficiency of TSH in reproducing decoherence proves that we can observe splitting without decoherence. Despite this last observation we find interesting to look at the splitting of the nuclear density not only in configuration space, but also in momentum space. The position representation seems indeed more natural, due to the fact the BO states are only defined “at fixed nuclear positions” and not “at fixed nuclear momenta”. In Fig. SM.4 we show the splitting of the nuclear density in momentum space, which is perfectly captured by the momentum distribution of the classical trajectories.



Supplemental Material, Figure SM.4. Splitting of the nuclear density in momentum representation (line), compared with quantum-classical results (histogram).

### Computational cost of the CT-MQC scheme

The actual bottleneck of trajectory-based approaches to non-adiabatic dynamics is the computation of electronic structure properties. However, the solution of the full quantum problem requires to treat the nuclei quantum-mechanically and indeed here a trajectory-based method is able to cut the computational cost.

For instance, we have compared in the proton-coupled-electron-transfer problem the computational cost needed to solve the TDSE with the CT-MQC equations. The TDSE is integrated using split-operator-technique, referenced in the Supplemental Material, while the electronic and nuclear equations of the CT-MQC scheme are solved with the fourth-order Runge-Kutta algorithm and velocity-Verlet algorithm, respectively. In these particular cases, quantum mechanical calculations require a smaller integration time-step than the quantum-classical method, i.e. 5 times smaller for the case shown in the Letter. Solving the TDSE up to 1000 a.u. with  $1000 \times 1000$  grid points for one nucleus and one electron takes approximately 15 minutes on a normal desktop (Intel Core i7-4790 3.60 GHz), while it takes 1 minute for the CT-MQC with 200 trajectories. To perform the same

number of integration steps, the computational cost of the CT-MQC is approximately a factor 3 smaller than solving the TDSE.

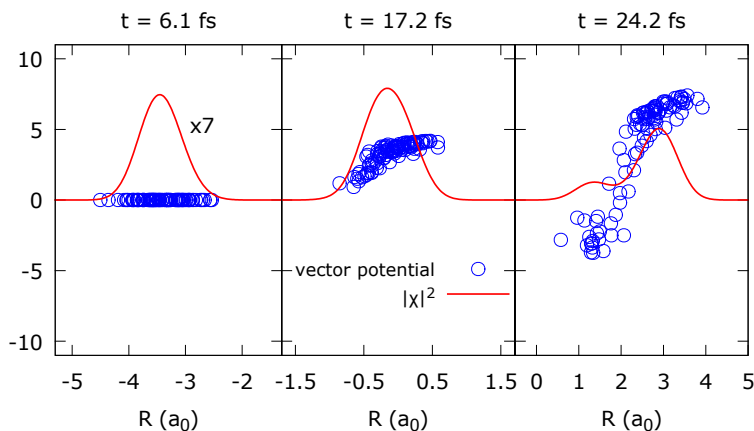
As for the scaling of the computational cost in going to higher dimensions, the numerical effort needed to include a larger number of trajectories, in order to appropriately sample the configurations space, scales linearly with the number of trajectories.

## TIME-DEPENDENT VECTOR POTENTIAL

The time-dependent vector potential of the theory is a gauge-dependent quantity. Exact quantum-mechanical results are presented in a gauge where the vector potential is set to zero (that is possible since the systems under considerations are solved in one-dimension). In order to propose a CT-MQC procedure as general as possible, we have chosen to work in a different gauge when developing the algorithm, namely

$$\epsilon_0^{(I)}(t) + \epsilon_{\text{TD}}^{(I)}(t) + \sum_{\nu} \mathbf{V}_{\nu}^{(I)} \cdot \mathbf{A}_{\nu}^{(I)}(t) = 0 \quad (\text{SM.22})$$

Therefore, as an example, we show in Fig. SM.5 the vector potential calculated within the CT-MQC scheme for model case (1). It cannot be compared with exact results, as it is identically zero in the quantum case. This is also the reason why the only potential shown in the Letter is the gauge-invariant part of the TDPES. The vector potential is non-



Supplemental Material, Figure SM.5. Snapshots of the vector potential taken along the quantum-classical evolution.

zero only after the nuclear density splits in two branches. Notice that it appears as a nuclear momentum correction, due to the non-adiabatic nature of the electrons, in the nuclear Hamiltonian in Eq. (2) of the Letter. At time  $t = 24.2$  fs in Fig. SM.5, the vector potential contributes a negative term only to those trajectories that move on the upper BO surface, as its negative part corresponds to the region occupied by the BO-projected wave packet “on” the upper BO surface. The opposite situation applies to the positive part of the vector potential. This observation is in agreement with previous analysis reported in Ref. [3].



- 
- [1] A. Abedi, F. Agostini, Y. Suzuki, and E. K. U. Gross, *Phys. Rev. Lett* **110**, 263001 (2013).
- [2] F. Agostini, A. Abedi, Y. Suzuki, and E. K. U. Gross, *Mol. Phys.* **111**, 3625 (2013).
- [3] F. Agostini, A. Abedi, Y. Suzuki, S. K. Min, N. T. Maitra, and E. K. U. Gross, *J. Chem. Phys.* **142**, 084303 (2015).
- [4] F. Agostini, S. K. Min, and E. K. U. Gross, *Ann. Phys.* , Doi: 10.1002/andp.201500108 (2015).
- [5] S. Shin and H. Metiu, *J. Chem. Phys.* **102**, 23 (1995).
- [6] A. Abedi, F. Agostini, and E. K. U. Gross, *Europhys. Lett.* **106**, 33001 (2014); F. Agostini, A. Abedi, and E. K. U. Gross, *J. Chem. Phys.* **141**, 214101 (2014).
- [7] M. D. Feit, F. A. Fleck Jr., and A. Steiger, *J. Comput. Phys.* **47**, 412 (1982).
- [8] J. C. Tully, *J. Chem. Phys.* **93**, 1061 (1990).